Nanoscale

RSC Publishing

PAPER

Microwave dielectric heating of non-aqueous droplets in a microfluidic device for nanoparticle synthesis†

Cite this: *Nanoscale*, 2013, **5**, 5468

Dorota Koziej,*[ab] Caspar Floryan,[a] Ralph A. Sperling,[a] Allen J. Ehrlicher,[a] David Issadore,[cd] Robert Westervelt[a] and David A. Weitz[a]

Received 28th January 2013
Accepted 4th April 2013

DOI: 10.1039/c3nr00500c

www.rsc.org/nanoscale

We describe a microfluidic device with an integrated microwave heater specifically designed to dielectrically heat non-aqueous droplets using time-varying electrical fields with the frequency range between 700 and 900 MHz. The precise control of frequency, power, temperature and duration of the applied field opens up new vistas for experiments not attainable by conventional microwave heating. We use a non-contact temperature measurement system based on fluorescence to directly determine the temperature inside a single droplet. The maximum temperature achieved of the droplets is 50 °C in 15 ms which represents an increase of about 25 °C above the base temperature of the continuous phase. In addition we use an infrared camera to monitor the thermal characteristics of the device allowing us to ensure that heating is exclusively due to the dielectric heating and not due to other effects like non-dielectric losses due to electrode or contact imperfection. This is crucial for illustrating the potential of dielectric heating of benzyl alcohol droplets for the synthesis of metal oxides. We demonstrate the utility of this technology for metal oxide nanoparticle synthesis, achieving crystallization of tungsten oxide nanoparticles and remarkable microstructure, with a reaction time of 64 ms, a substantial improvement over conventional heating methods.

Introduction

The properties of nanoparticles differ from those of their bulk counterparts due to the confinement effect caused by their size, structure, and shape.[1] To optimize these properties for specific applications it is useful to carry out synthetic reactions with small volume and low cost. Microfluidic reactors are valuable tools for this application, due to their ability to rapidly dose reagents and to create homogenous mixtures on the scale of microns.[2–7] Microfluidic systems can be used either in continuous flow or segmented flow through the use of droplets. The use of segmented flow reactors, in comparison with their continuous counterparts, allows nanoliter volumes of reaction solutions to be independently controlled with precise reaction conditions, such as heat, mass transfer rates, and temperature.[2–7] The ability to separate and control the stages of nucleation and growth is a unique aspect of microfluidic synthesis. These properties found broad application in fabrication of metal,[8] III–VI semiconductor[5] and polymeric[9] nanoparticles with defined size and structure. Recent developments have been directed toward scaling out of the processes by adding reactors working in parallel.[10,11] Despite enormous progress in using microfluidic reactors for the synthesis of nanoparticles, the crystallinity of metal oxide nanoparticles has only been demonstrated in systems where the reactants are maintained at high temperatures for at least 1 to 30 minutes. This can be accomplished through the use of a resistive heater, an oil bath or an oven, which heats either the entire device, or just the collection tube.[4,12] An alternate means of efficiently increasing the temperature is to heat the sample alone. This can be done through the use of microwaves, which selectively and directly heat the sample itself.[12–14] Microwave heating can significantly increase the rate of synthesis of metal oxide nanoparticles in the bulk, reducing the reaction time from hours to minutes.[15]

Recently, we have shown that microwave heating can be integrated into droplet based microfluidic chips, enabling rapid (<30 ms) heating to temperatures 30 °C above the base temperature.[16] In this previous study, we heated water at $f = 2.4$ GHz, utilizing its large dielectric resonance loss at microwave frequencies. Several novel device geometries and materials have been employed to fabricate the efficient

[a]*School of Engineering and Applied Sciences, Department of Physics, Harvard University, Cambridge, MA 02138, USA. Tel: +1 61 7496 9788*

[b]*ETH Zürich, Department of Materials, Laboratory for Multifunctional Materials, 8093 Zurich, Switzerland. E-mail: koziejd@mat.ethz.ch; Fax: +41 14 633 15 45; Tel: +41 14 4633 6055*

[c]*Center for Systems Biology, Massachusetts General Hospital, Boston, MA 02114, USA*

[d]*Department of Bioengineering, School of Engineering and Applied Science, University of Pennsylvania, Philadelphia, Pennsylvania, USA*

† Electronic supplementary information (ESI) available: Optical images of the microfluidic device; measurements of dependence of the microwave frequency on the temperature of benzyl alcohol droplets; a summary of dielectric properties of common solvents; a quasi-static electrical field simulation; TEM, HRTEM and SEAD of nanoparticles washed with ethanol. See DOI: 10.1039/c3nr00500c

transmission of microwave power to samples on microfluidic chips.[17,18] Because the research on microfluidic-microwave reactors has been driven by its potential application for DNA amplification or cell lysis, the state-of-the-art devices are dedicated to heating of water in the frequency range between 2.45 and 15 GHz. However, water is not a suitable solvent for the low temperature synthesis of many inorganic metal oxides in crystalline states. Instead solvents such as benzyl alcohol are utilized, since in the bulk they enable both rapid microwave synthesis and efficient crystallization at relatively low reaction temperatures.[15] Despite the widespread use of microwave heating in the synthesis of nanoparticles, microwave heating has never been done with a microfluidic device and the advantages of this technique have not been explored.

In this paper we describe a microfluidic dielectric-heating device, operating at 700–900 MHz, which is capable of precisely heating the non-aqueous solvents used for nanoparticles synthesis, for instance benzyl alcohol, *n*-butanol and ethylene glycol.[19–23] Label-free IR temperature imaging provides quantitative information about the dielectric heating of the benzyl alcohol droplets, heat transfer from the droplets, and non-dielectric losses. Additionally we measure with high temporal resolution the dielectric heating of the benzyl alcohol droplets by fluorescence imaging. To demonstrate the utility of this approach, we synthesize crystalline tungsten oxide nanoparticles in benzyl alcohol using our chip. Typically tungsten oxide synthesis leads to a $WO_3 \cdot nH_2O$ product in the form of platelets independent of the heating method.[24,25] Tungsten oxides nanoparticles have been widely used materials for application in gas sensing, water splitting, electrochromic windows. In addition, unconventional applications of tungsten oxide nanoparticles are for high Tc superconductors, field emission displays and optical recording devices.[26–29] Therefore, we choose this material to show the feasibility of microwave synthesis on a microfluidic chip.

Materials and methods

Device

The microfluidic device is fabricated using standard soft lithography. The PDMS channels are 50 μm high. The device was plasma bonded to a thin glass slide (0.13 mm), the channels were functionalized with Aquapel and baked for 20 minutes at 60 °C. The electrodes are fabricated by applying a low-melting solder fill technique previously described.[30] The electronics to generate the microwave power at 700–900 MHz is assembled similar to the electronics for 3 GHz frequency.[16] The microwaves are generated with a voltage-controlled oscillator (ZX95-1200W+, Mini-Circuits) and are amplified with a power amplifier (ZHL-211-8 Mini-Circuits). The quasi-static simulation of the electrical field between the electrodes is performed with Ansoft, Maxwell software.

Calibration of temperature measurements

We use rhodamine B (RhB) and rhodamine 110 (Rh110) at a concentration of 0.1 mmol and measure the emission spectra on a Leica TCS SP5 confocal microscope equipped with a heating stage (Warner Instruments). The dyes are excited at 488 nm and the emission is examined by scanning in 5 nm steps between 500 and 650 nm at different temperatures. The two dyes have different temperature-dependent spectra when excited at 488 nm allowing the individual signal to be separately measured and the temperature of the sample determined by calibration.

Single droplet temperature measurement set-up

The detection setup consists of a 50 mM, 488 nm cw laser coupled into the backport of a Motic AE-31 fluorescence microscope. The laser is focused by a 40×, NA 0.85 objective into the flow channel of the microfluidic device, which is heated by microwaves. The emitted fluorescence is collected by the same objective and passed through a series of dichroic mirrors at the back of the microscope. Photomultiplier tubes behind the bandpass filter detect the light at 536/40, data acquisition is carried out on a PC with a FPGA card from National Instruments and a LabView program.

Thermal IR imaging

The temperature profile of the device is measured with an IR camera SC 5600 FLIR equipped with an InSb detector using a frame rate 100 Hz. The 0.13 mm thick glass slide is partially transparent to infrared; therefore we cannot image completely through the glass and measure temperature directly in the channel. In the detector spectral range (3–5 μm) the transmittance of glass lies between 90 and 40%.

Chemicals

Anhydrous benzyl alcohol (≥99%), tungsten hexachloride (≥99.9%), rhodamine B (97%), and rhodamine 110 (≥99.0%), oxalyl chloride (98%), poly(propylene glycol)-*block*-poly(ethylene glycol)-*block*-poly(propylene glycol) bis(2-aminopropyl ether), anhydrous dichloromethane (99.8%) were supplied by Sigma-Aldrich, Fluorinert Electronic Liquid FC-40 (FC-40 oil) and HFE-7100 by 3 M, polyethylene oxide, M_w 100 000 by Alfa Aesar, Krytox 157 FSH by Miller-Stephenson.

All chemicals were used without further purification. SU8 3050 was purchased from MicroChem, polydimethylsiloxane (PDMS) prepolymer and curing agent – Sylgard 184 – were from Essex Brownell, indium alloy Ind19 (52In, 32.5 Bi, 16.5 Sn) 0.020″ diameter was from Indium Corporation, Aquapel was from Pittsburgh Glass Works, LLC.

Synthesis in a microfluidic device

Tungsten hexachloride (20 mg) was added, in an oxygen- and water-free atmosphere, to anhydrous benzyl alcohol (3 ml). The light blue solution was directly transferred to a glass syringe. The surfactant to stabilize benzyl alcohol droplets in FC-40 oil was synthesized according to the published procedure.[31] Then, 1 wt% of surfactant was dissolved in FC-40 and the resulting solution was filtered and transferred to a glass syringe. The liquids were injected into the channels using syringe pumps

from Harvard Apparatus. The experiments were performed at a constant flow rate of benzyl alcohol at 20 μl h^{-1} and the oil at 120 μl h^{-1}, unless otherwise stated. After heating the droplets in a microfluidic-microwave device the solution turned from transparent bluish to slightly yellowish. In the control experiments, the reaction solution was heated in a CEM Explorer laboratory microwave reactor in a 10 ml vessel (7.5 ml reaction solution) at 60 °C for 1–30 minutes and at 120 °C for 10 minutes. At 60 °C (1 to 15 minutes) of reaction we did not observe formation of precipitate even after the solution was centrifuged for several hours at a speed of 15 000 rpm.

Synthesis of poly(perfluoropropylene glycol)–PEG

Krytox 157 FSH is a perfluorinated polyether with a carboxylic group at one end. The carboxylic group is converted to the acid chloride by reacting it with an excess of oxalyl chloride. After evaporating off the excess of oxalyl chloride, a diamine PEG is added. The acid chloride of the fluorinated block reacts with the amino groups of the PEG, forming di- and triblock molecules. Unreacted PEG is separated by centrifugation; evaporation of the solvent yields the surfactant that can be used without further purification.

Material characterization

Transmission Electron Microscopy (TEM) and high-resolution Transmission Electron Microscopy (HR-TEM) investigations were performed on a Philips Tecnai F30 at 300 kV. Scanning Electron Microscopy (SEM) studies were performed on a Zeiss FESEM Supra55VP at 5 kV. The droplets drip directly from the collection tube of the PDMS device onto carbon-coated copper grids (TEM) or the alumina stub (SEM) were immediately vacuum dried. X-ray powder diffraction (XRD) was measured using a Panalytical XPert Pro Diffractometer (45 kV, 40 A) equipped with an X'cellerator detector and fixed slits. The repeated-scans at 2 theta from 10 to 60° were merged to improve the signal-to-noise ratio.

Results and discussion

Device for microwave heating of non-aqueous solvents

Our droplet based micro-reactor was fabricated from PDMS using soft lithography and consists of a droplet maker followed by a microwave heater as schematically illustrated in Fig. 1 and shown in ESI Fig. S1,† The droplet maker is in the flow focusing geometry, with inlets that are each 20 μm wide and a nozzle that smoothly widens from 20 μm to 50 μm. Microwave power is locally delivered by indium-alloy electrodes that are directly integrated into the microfluidic device[16,30] and are situated 0.5 cm downstream from the droplet maker. The frequency of the rotational relaxation process of benzyl alcohol molecules is approximately 850 MHz.[20] In order to efficiently generate heat the frequency of the heater should approximately match with that of benzyl alcohol. At 2.45 GHz the molecules of benzyl alcohol are not able to follow the electrical field oscillation and behave like a less-polar solvent. Therefore a device designed to heat water with microwave heating using frequency 2.45 GHz (400 mW) is not efficient for heating of benzyl alcohol. Conventional laboratory microwave ovens compensate for the low energy absorption of non-aqueous solvents at 2.45 GHz by using high output power. Instead for our experiments, we construct an inexpensive microwave source that can supply up to 800 mW in the frequency range between 700 and 900 MHz. Although, we test this device at different frequencies with benzyl alcohol (see ESI Fig. S2†), it can also be used without further modification with other common non-aqueous solvents for nanoparticle synthesis.[21–23,32] For example 1-hexanol, 1-butanol, 2-propanol, glycerol and diethylene glycol all have higher relaxation times (τ) than that of water and therefore their maximal dissipation factors (δ) are below 2.45 GHz (Table S1, ESI†). The microwave power is controlled by varying the peak-to-peak voltage of the amplifier, and the frequency is controlled by a voltage controlled oscillator. We match the impedance of the electrodes to that of the source and optimize the electrodes geometry to ensure efficient delivery of microwave power to the droplets; we model the quasi-static electrical field to help optimize the device (see ESI, Fig. S3†). As a fluid we use FC-40 3M oil with 1 wt% Krytox–PEG surfactant[31] for the continuous phase and benzyl alcohol for the dispersed phase.

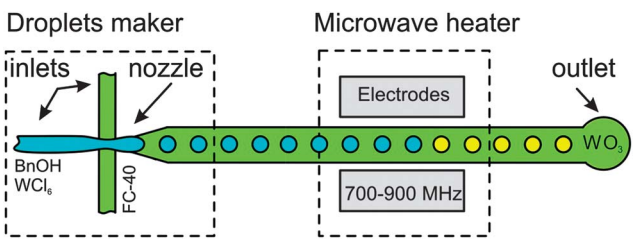

Fig. 1 Schematic of the microfluidic device. The flow-focusing droplet maker is followed by a microwave heater. The benzyl alcohol droplets are rapidly heated using microwaves of 862 MHz frequency (7.5 V tuning voltage). Each droplet is a micro-reactor for ultra-fast nanoparticle synthesis; one example is tungsten oxide.

Temperature within the benzyl alcohol droplets

To determine the temperature within the droplets we measure the fluorescence intensity of dyes dissolved in the benzyl alcohol. We first calibrate the temperature dependence of the fluorescence intensity of rhodamine B and 110, since little is known about their behavior in benzyl alcohol.[33,34] Interestingly, the fluorescence intensity of each dye decreases linearly with temperature; this is unlike the behavior in water where only RhB is temperature dependent.[35,36] The measured temperature sensitivities of RhB at 575 nm and Rh110 at 530 nm are very similar and are 1.75 ± 0.08%/°C and 1.74 ± 0.08%/°C, respectively (see ESI Fig. 4 and 5†). Further, we measure the fluorescence intensity from both dyes in droplets of benzyl alcohol in the microfluidic chip, and use this to determine the temperature within the droplets when they are heated with the microwaves. Fluorescence is excited by a 488 nm, 50 mW laser that is focused on the droplets when they are in the flow channel, between the electrodes used for the microwave heating. The fluorescence emitted from each individual droplet is collected by a microscope objective and guided through a series of dichroic mirrors to three photomultiplier tubes. We record the

fluorescence intensity of many droplets as a function of the peak voltage applied to the microwave heater, and determine the average over one thousand equally sized droplets. To ensure the accuracy of the results we pick the equally sized droplets from the whole population of droplets by setting the lower limit of fluorescence detection and the duration of droplets, as shown in the ESI, Fig. 6.†

In contrast to long-exposure fluorescence imaging of many drops traveling through the microwave heater,[37–39] this method does not require sophisticated background extraction and perfectly equally sized drops. The temperature rises linearly with microwave power, which is proportional to the square of the peak voltage applied to the electrodes, as shown in Fig. 2. The maximum temperature of the droplets is 50 °C which represents an increase of about 25 °C in 15 ms. Interestingly, when we compare the temperature of droplets different in size, we can distinguish two regimes; for droplets smaller than the size of the channel, the slope of the temperature increase with microwave power is steeper and the maximum temperature is higher than that for the larger droplets. Because the larger droplets are deformed by the walls and therefore in close proximity to the PDMS, heat is more efficiently conducted to the bulk of the device; in contrast the carrier oil has a low thermal conductivity (κFC-40 0.065 W m^{-1} C^{-1})[40] which, in the case of smaller droplets, effectively prevents dissipation of heat from the droplets into the device. The standard deviation of temperature (σ_T) is equal to 1.5 °C for smaller droplets, and 0.8 °C for larger droplets. The error in the temperature measurements comes from the variation of the vertical position of droplets smaller than the channel height, which has an impact on the focal point and thus on the fluorescence intensity.

Evaluation of dielectric and non-dielectric heating

There is an ongoing debate whether the enhancement of chemical reactions driven by microwave irradiation is due to rapid heating or selective interaction of the electromagnetic field with polar molecules. Our microfluidic-microwave droplet heater, due to its ability to separate conventional heat transfer mechanisms from dielectric heating,[41] can help shed light onto these questions. To separate the effects of conventional heating from dielectric heating, we utilize infrared imaging to visualize the heat distribution through the device. To directly evaluate the influence of the carrier oil on the heat transfer from the droplets, we measure the temperature distribution on the glass surface of the device using an IR camera. The camera is calibrated to determine the temperature in the images, which is reflected by the color map.

We collect images at a rate of 100 Hz using an integration time of 2.2 ms, allowing us to monitor the change in the temperature of the glass surface as the device heats up when a peak voltage of 8.85 V is first applied to the microwave heater. However, what we essentially measure is the amount of heat vertically dissipated to the substrate from the droplets as the microwave is turned on. The IR images show that the device heats up in the region below which the microwaves are applied over the course of about 15 s, as illustrated in Fig. 3a. We extract the time evolution of the lateral temperature profiles of the heater and we find that the temperature gradient is established on the length of 0.5 cm when the steady state is reached as shown in the inset of Fig. 3. Even after just 10 ms the temperature of the glass directly below the microwave heater clearly begins to increase; after 500 ms we can measure the heat dissipated also in horizontal directions. Steady state conditions are established after 15 s and the temperature of the device remains constant over several hours of continuous operation. This temperature gradient shows that the benzyl alcohol

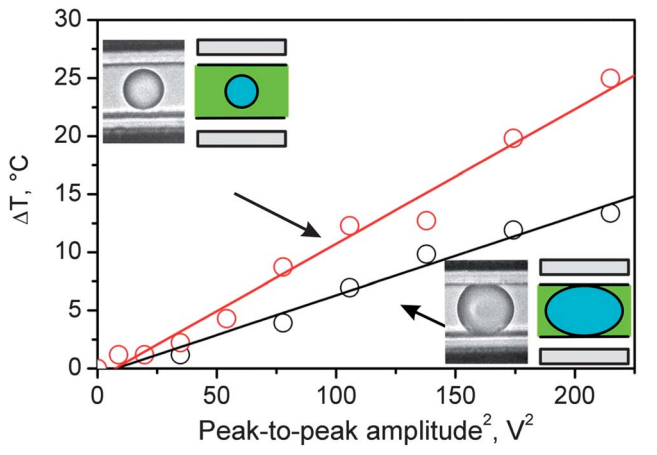

Fig. 2 The temperature change of the droplets as a function of the peak-to-peak voltage. The red curve represents droplets smaller than the channel, formed at a 20 ml h^{-1} flow rate of benzyl alcohol. The black curve represents droplets larger than the channel, which are compressed by the channel; they are formed at a 50 ml h^{-1} flow rate of benzyl alcohol. The flow rate of oil is kept constant at 120 ml h^{-1}. The baseline temperature is 25 °C.

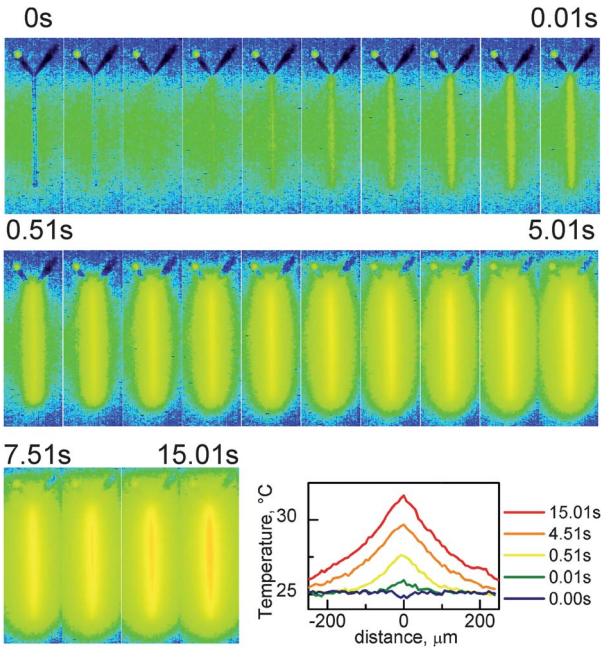

Fig. 3 IR image sequence of microwave heating taken at 100 frames per second. Inset bottom, right – the temperature profile as a function of distance from the center of the channel.

droplets are hotter than their surroundings, thus verifying dielectric heating.[16–18]

To quantitatively determine the heat losses, we measure the temperature of the device when it reaches steady state. We determine the temperature profiles along the channel from the IR images. We observe an abrupt increase in the temperature at the entrance of the microwave heater and a corresponding abrupt decrease at the exit; the temperature remains constant along the heated area. Adjusting the applied microwave voltage from 0 to 13.2 V peak-to-peak changes the temperature from 25 to 45 °C as shown in Fig. 4a and b. This represents an increase of 20 °C, somewhat less than that of the drops themselves. To differentiate microwave heating of the fluid from resistive heating we remove the benzyl alcohol from the device and flow only non-absorbing fluorinated oil (FC-40). In this case, there is very little temperature change measured, as the device only heats up by a maximum of 5 °C as shown in Fig. 4c; this residual temperature rise can be attributed to traces of resistive heating, which may come from artifacts such as electrode imperfections.

Honeycomb-like microstructure made of nanoparticles

The ability to rapidly deliver power to the non-aqueous droplets using dielectric heating offers new opportunities to synthesize inorganic materials. To illustrate this potential, we use our microfluidic microwave heater to synthesize tungsten oxide nanoparticles within benzyl alcohol droplets using the synthesis protocol for a conventional reaction in oil bath described by Niederberger *et al.*[24] We use the microwave-microfluidic device described above to generate droplets of tungsten hexachloride and benzyl alcohol solution in FC-40 oil. The droplets of *ca.* 50 μm reside in the area exposed to dielectric heating of 50 °C for 64 ms. An example of droplets and their assembly after evaporation of FC-40 is shown in Fig. 5. After drying in air, and without further washing, the unique honeycomb-like microstructure is formed. If the structure is dried onto the polished Si-wafer in a vacuum, the honeycomb-like microstructure is only partially preserved. Most likely the poor adhesion between the dried droplets and the Si substrate results in the partial exfoliation of the microstructure under vacuum (Fig. 6a). A closer look at the dried droplets shows that there is more solid phase collected at the boundaries between the droplets than in the middle of the single droplet. Additionally, a wrinkled microstructure inside the droplets is observed (Fig. 6b). TEM images not only confirm the morphology of the dried droplets but also reveal a subtle nanostructure. The darker regions inside the droplets, clearly visible already in the SEM image as wrinkles, and the edges of the droplets consist of assemblies of primary nanoparticles (Fig. 7a–c).

Inside the droplets the individual nanoparticles are observed. HR-TEM images deliver the final proofs of their crystallinity (Fig. 7d–f). The size of primary particles does not exceed 3 nm. The XRD pattern shows broad reflections typical

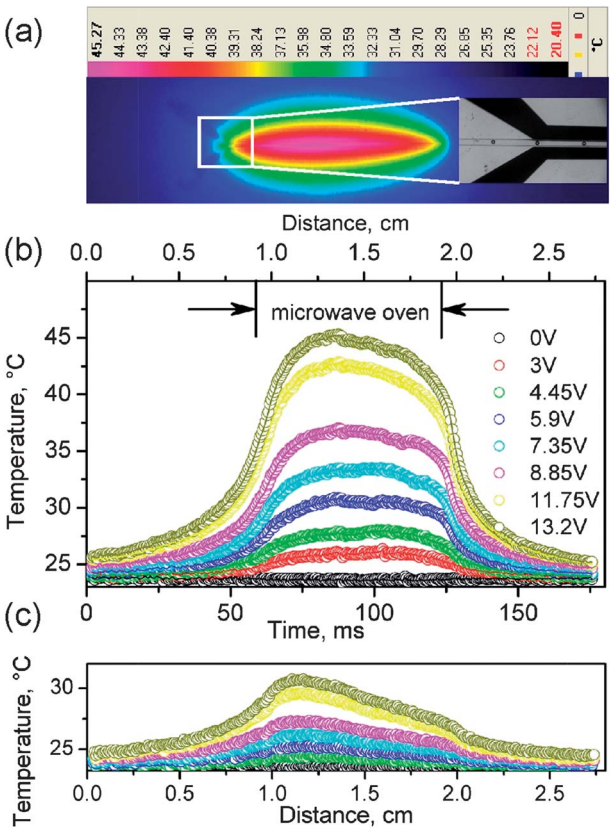

Fig. 4 (a) Two-dimensional temperature map of heat dissipation at the surface of a microfluidic-microwave heater. In the inset is shown an optical image of the droplets entering the microwave heater area, (b) temperature profiles along the channel at different peak-to-peak voltages in the presence of microwave-absorbing benzyl alcohol droplets, and (c) corresponding background temperature profiles when only the non-absorbing FC-40 oil is flowing.

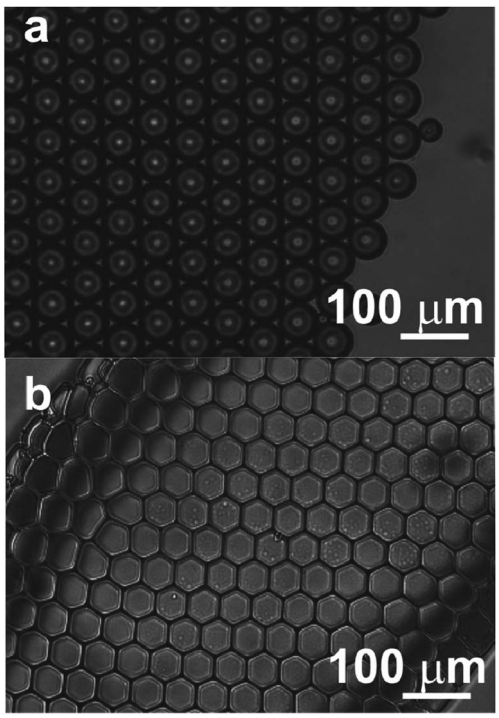

Fig. 5 Optical microscopy images of a single monolayer of benzyl alcohol droplets: (a) benzyl alcohol droplets immerse in the continuous FC-40 phase self assemble onto a glass surface, (b) after the continuous phase (FC-40) evaporates the droplets are still stable and adapt a honeycomb-like microstructure.

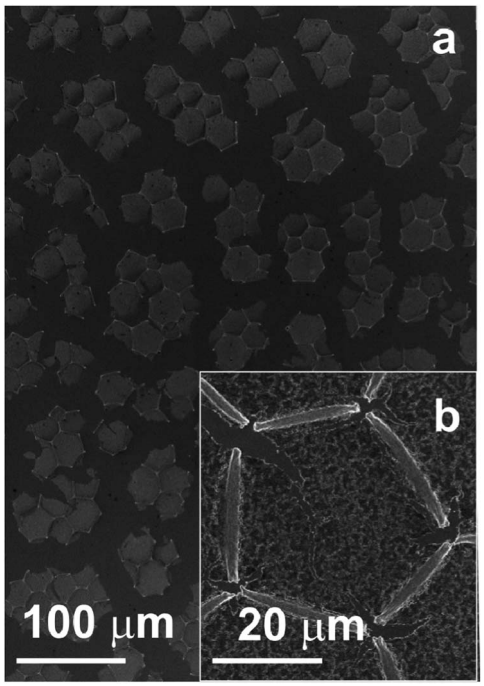

Fig. 6 SEM images of dried droplets at different magnifications, which show (a) a partially preserved honeycomb-like microstructure, and (b) wrinkle-like features inside the droplets.

for nanoparticles that complicates an unambiguous identification of the crystal structure. However, the best match among different tungsten oxide hydrates ($WO_3 \cdot nH_2O$, $n = 0$, 0.33, 0.5, 1 and 2) is obtained with orthorhombic tungsten oxide 0.3-hydrate, ICDD Nr. 01-072-0199 (Fig. 8). Interestingly, the size of nanoparticles and their structure change if they are washed with ethanol, which can be observed in the sharp reflection in the XRD pattern (Fig. 8b). Also in the HR-TEM image individual 2 nm nanoparticles cannot be distinguished anymore, but rather nanoparticles of 10 nm and their agglomerates (ESI Fig. S7†). The diffraction rings in the corresponding electron diffraction (ED) pattern are characteristic of polycrystalline materials. The sharp reflections in XRD and SEAD patterns can be attributed to the tungstate oxide hydroxide nanoparticles (Fig. 8b).

It is likely that benzyl alcohol not only acts as a reaction medium, but also as a capping agent. By washing with ethanol, the organic residuals are removed from the surface of tungsten oxide hydrates. We believe the growth process is driven by the decrease in total system energy by reducing the surface energy. Furthermore, heating by irradiation with an electron beam accelerates nanoparticle transformation and growth. This is visualized by consecutive recording of the diffraction patterns at the same spot. We observe a successive transformation of the diffraction rings (ESI Fig. 7a†) into well-developed lattice planes

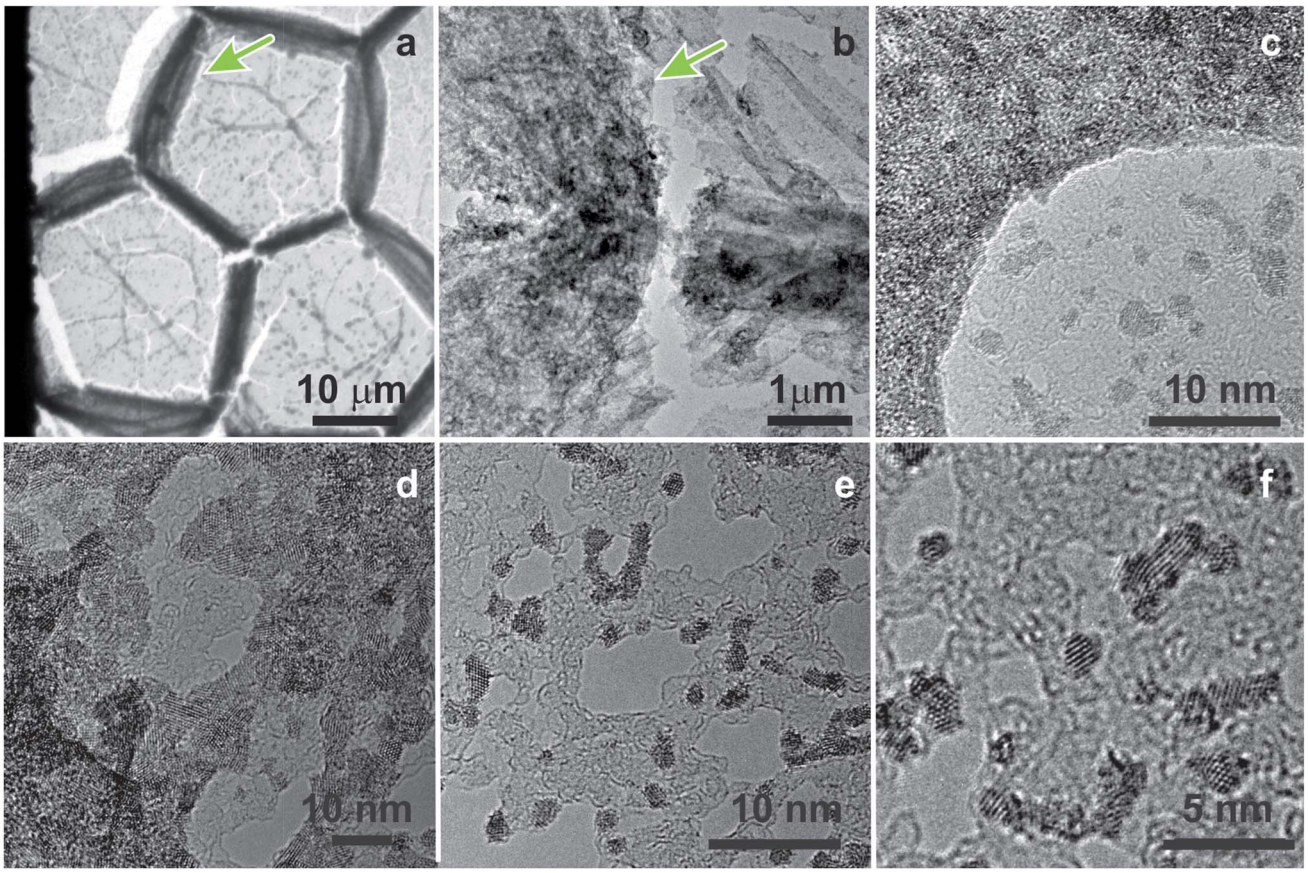

Fig. 7 TEM and HR-TEM images of dried droplets. Green arrow points the spot, which is magnified in the following image (from a to c). The nanoparticle agglomerates do not exhibit preferential crystallographic orientation.

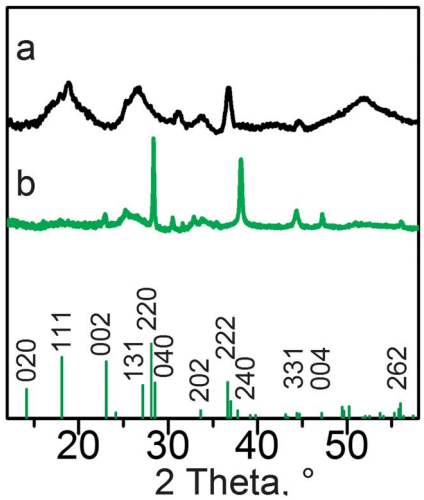

Fig. 8 XRD patterns of the reaction product: (a) without washing, (b) after washing with ethanol. The sharp reflections are due to anisotropic growth. Vertical green bars at the bottom: reference pattern of $WO_3 \cdot 0.33H_2O$, ICDD no. 01-072-0199.

(ESI Fig. 8†). It is not surprising since benzyl alcohol is known to stabilize small nanoparticles and metastable crystal structures.[32,42] For instance, we have shown that benzyl alcohol can stabilize 1–2 nm large MoO_2 nanoparticles in the hexagonal crystal structure. If acetophenone is added to the reaction solution, the nanoparticles grow through oriented attachment and transform into the thermodynamically more stable monoclinic phase. Also the role of electron beam irradiation in oriented attachment and growth of nanoparticles was recently visualized by real-time HR-TEM imaging of the growth of Pt_3Fe and growth of Au nanoparticles at the surface of CdSe.[43,44] In the case of Au on CdSe Meyns *et al.* showed that during irradiation of the sample by the electron beam, the thin shell of Au at the surface of CdSe nanoparticles evolved into dot-like deposits with high contrast.[44] The authors suggest that it can be correlated with the lower degree of coverage with ligands at the surface of CdSe. Whereas in the case of Pt_3Fe the observations revealed the growth of winding polycrystalline nanoparticle chains by shape-directed nanoparticle attachment followed by straightening and orientation and shape corrections to yield single-crystal nanorods.[43]

Finally, we performed the control bulk experiments in the laboratory microwave reactor at 60 °C and 120 °C (see ESI Fig. S9†). The XRD pattern of nanoparticles synthesized at 120 °C over 10 minutes can be clearly assigned to the $WO_3 \cdot H_2O$ crystal structure (ICDD no. 00-018-1418). At 60 °C we did not observe nanoparticle formation at reaction times shorter than 15 minutes. Even though the corresponding XRD pattern shows very broad reflections it can also be assigned to $WO_3 \cdot H_2O$.

The nanoparticles synthesized in the microwave-microfluidic device adopt the $WO_3 \cdot 0.33H_2O$ crystal structure in contrast to $WO_3 \cdot H_2O$ obtained in our control synthesis in the laboratory microwave reactor and experiments in oil bath.[24,25] At the same time the reaction time is decreased from 15 minutes at 60 °C in a bulk laboratory microwave reactor down to only 64 ms in a microfluidic device, demonstrating the advantages of this approach. While most previous studies focus on the engineering of the tungsten oxide nanoparticles, wires and their subsequent assembly,[27–29] our technique offers a route to simultaneously synthesize and assemble the nanoparticles. Recently, a versatile and simple approach to produce tailor-made hierarchical porous materials was presented.[45] Using a microfluidic device to produce monodisperse templating droplets of tunable size, the materials with up to three levels of hierarchy were prepared. Adding the microwave-reactor to the microfluidic chip could additionally give a control on the chemical composition of porous structures.

Conclusions

Although microfluidic reactors are often applied to synthesize crystalline nanoparticles, microwave heating has not previously been utilized. Here we show that with microwave heating of pL-sized droplets we can produce appropriate conditions to crystallize inorganic metal oxide nanoparticles. This technique enables future work to alter the concentration of the precursor and the heating time of the droplets, to finely control the assembly of nanoparticles within each droplet. The use of our microfluidic chip leads to drastically reduced synthesis time (from 15 minutes in a bulk microwave reactor, down to 64 ms in a microfluidic device). Additionally, our chip has the potential to help address the important issue of distinguishing the effects of non-thermal and thermal effects of microwave irradiation in microwave driven particle synthesis.[19] The two main constraints in addressing this question are: the limited compatibility of the standard laboratory microwave reactor with spectroscopic equipment; and the low temporal resolution of most of the available spectroscopic techniques. With the help of single droplet fluorescence detection and infrared thermal imaging techniques we can ensure that heat is generated only due to dielectric heating of benzyl alcohol. Therefore, in future, a droplet-based microfluidic system can provide a valuable platform for coupling of a dielectric heating and *in situ* spectroscopy techniques. Moreover, a unique advantage of the application of spectroscopic techniques to a microfluidic chip is the spatial resolution, which can be translated into the enhanced temporal resolution without loss of data quality.[46,47] Hence, these results reported help assess the utility of microfluidic microwave heating for exceptionally fast inorganic material synthesis.

Acknowledgements

This work was supported by the NSF (DMR-1006546) the Harvard MRSEC (DMR-0820484), the Swiss National Foundation, projects: PA00P2 129086 and 2-77354-12 and by the Electron Microscopy of ETH Zurich (EMEZ). Martin Süess (EMEZ) help with HR-TEM and Rahel Boehlen support with the soft-litography are greatly acknowledged. DK thanks Prof. Markus Niederberger (ETH Zurich) for his enthusiastic support.

Notes and references

1 A. P. Alivisatos, *Science*, 1996, **271**, 933–937.
2 J. Il Park, A. Saffari, S. Kumar, A. Günther and E. Kumacheva, *Annu. Rev. Mater. Res.*, 2010, **40**, 415–443.
3 A. J. deMello, *Nature*, 2006, **442**, 394–402.
4 A. Abou-Hassan, O. Sandre and V. Cabuil, *Angew. Chem., Int. Ed.*, 2010, **49**, 6268–6286.
5 E. M. Chan, A. P. Alivisatos and R. A. Mathies, *J. Am. Chem. Soc.*, 2005, **127**, 13854–13861.
6 S.-A. Leung, R. F. Winkle, R. C. R. Wootton and A. J. deMello, *Analyst*, 2005, **130**, 46–51.
7 I. Shestopalov, J. D. Tice and R. F. Ismagilov, *Lab Chip*, 2004, **4**, 316–321.
8 Y. Song, H. Modrow, L. L. Henry, C. K. Saw, E. E. Doomes, V. Palshin, J. Hormes and C. S. S. R. Kumar, *Chem. Mater.*, 2006, **18**, 2817–2827.
9 S. Xu, Z. H. Nie, M. Seo, P. Lewis, E. Kumacheva, H. A. Stone, P. Garstecki, D. B. Weibel, I. Gitlin and G. M. Whitesides, *Angew. Chem., Int. Ed.*, 2005, **44**, 724–728.
10 A. Aimable, N. Jongen, A. Testino, M. Donnet, J. Lemaitre, H. Hofmann and P. Bowen, *Chem. Eng. Technol.*, 2011, **34**, 344–352.
11 W. Ehrfeld, V. Hessel and H. Lowe, *Microreactors: New Technology for Modern Chemistry*, Wiley-VCH, 2000.
12 A. M. Nightingale, S. H. Krishnadasan, D. Berhanu, X. Niu, C. Drury, R. McIntyre, E. Valsami-Jones and J. C. deMello, *Lab Chip*, 2011, **11**, 1221–1227.
13 B. F. Cottam, S. Krishnadasan, A. J. deMello, J. C. deMello and M. S. P. Shaffer, *Lab Chip*, 2007, **7**, 167–169.
14 Z. L. Xue, A. D. Terepka and Y. Hong, *Nano Lett.*, 2004, **4**, 2227–2232.
15 I. Bilecka and M. Niederberger, *Nanoscale*, 2010, **2**, 1358–1374.
16 D. Issadore, K. J. Humphry, K. A. Brown, L. Sandberg, D. A. Weitz and R. M. Westervelt, *Lab Chip*, 2009, **9**, 1701–1706.
17 J. Geist, J. J. Shah, M. V. Rao and M. Gaitan, *J. Res. Natl. Inst. Stand. Technol.*, 2007, **112**, 177–189.
18 J. J. Shah, S. G. Sundaresan, J. Geist, D. R. Reyes, J. C. Booth, M. V. Rao and M. Gaitan, *J. Micromech. Microeng.*, 2007, **17**, 2224–2230.
19 S. A. Galema, *Chem. Soc. Rev.*, 1997, **26**, 233–238.
20 B. Gestblom, *Chem. Phys. Lett.*, 1980, **74**, 333–336.
21 R. Harpeness and A. Gedanken, *Langmuir*, 2004, **20**, 3431–3434.
22 X. Hu, J. Gong, L. Zhang and J. C. Yu, *Adv. Mater.*, 2008, **20**, 4845–4850.
23 M. Tsuji, M. Hashimoto, Y. Nishizawa, M. Kubokawa and T. Tsuji, *Chem.–Eur. J.*, 2005, **11**, 440–452.
24 M. Niederberger, M. H. Bartl and G. D. Stucky, *J. Am. Chem. Soc.*, 2002, **124**, 13642–13643.
25 I. Olliges-Stadler, J. Stötzel, D. Koziej, M. D. Rossell, J.-D. Grunwaldt, M. Nachtegaal, R. Frahm and M. Niederberger, *Chem.–Eur. J.*, 2012, **18**, 2305–2312.
26 J. Polleux, A. Gurlo, N. Barsan, U. Weimar, M. Antonietti and M. Niederberger, *Angew. Chem., Int. Ed.*, 2006, **45**, 261–265.
27 H. Zheng, J. Z. Ou, M. S. Strano, R. B. Kaner, A. Mitchell and K. Kalantar-Zadeh, *Adv. Funct. Mater.*, 2011, **21**, 2175–2196.
28 M. Breedon, P. Spizzirri, M. Taylor, J. du Plessis, D. McCulloch, J. Zhu, L. Yu, Z. Hu, C. Rix, W. Wlodarski and K. Kalantar-zadeh, *Cryst. Growth Des.*, 2010, **10**, 430–439.
29 K. Kalantar-zadeh, A. Vijayaraghavan, M.-H. Ham, H. Zheng, M. Breedon and M. S. Strano, *Chem. Mater.*, 2010, **22**, 5660–5666.
30 A. C. Siegel, S. S. Shevkoplyas, D. B. Weibel, D. A. Bruzewicz, A. W. Martinez and G. M. Whitesides, *Angew. Chem., Int. Ed.*, 2006, **45**, 6877–6882.
31 C. Holtze, A. C. Rowat, J. J. Agresti, J. B. Hutchison, F. E. Angile, C. H. J. Schmitz, S. Koster, H. Duan, K. J. Humphry, R. A. Scanga, J. S. Johnson, D. Pisignano and D. A. Weitz, *Lab Chip*, 2008, **8**, 1632–1639.
32 G. Garnweitner and M. Niederberger, *J. Mater. Chem.*, 2008, **18**, 1171–1182.
33 K. G. Casey and E. L. Quitevis, *J. Phys. Chem.*, 1988, **92**, 6590–6594.
34 J. F. Lou, T. M. Finegan, P. Mohsen, T. A. Hatton and P. E. Laibinis, *Rev. Anal. Chem.*, 1999, **18**, 235–284.
35 S. Ebert, K. Travis, B. Lincoln and J. Guck, *Opt. Express*, 2007, **15**, 15493–15499.
36 J. Sakakibara and R. J. Adrian, *Exp. Fluids*, 1999, **26**, 7–15.
37 T. Robinson, Y. Schaerli, R. Wootton, F. Hollfelder, C. Dunsby, G. Baldwin, M. Neil, P. French and A. deMello, *Lab Chip*, 2009, **9**, 3437–3441.
38 D. Ross, M. Gaitan and L. E. Locascio, *Anal. Chem.*, 2001, **73**, 4117–4123.
39 R. Samy, T. Glawdel and C. L. Ren, *Anal. Chem.*, 2008, **80**, 369–375.
40 3M™ Fluorinert™ Electronic Liquid FC-40, http://www.solutions.3m.com, 2011.
41 D. Obermayer, B. Gutmann and C. O. Kappe, *Angew. Chem., Int. Ed.*, 2009, **48**, 8321–8324.
42 D. Koziej, M. D. Rossell, B. Ludi, A. Hintennach, P. Novak, J.-D. Grunwaldt and M. Niederberger, *Small*, 2011, **7**, 377–387.
43 H.-G. Liao, L. Cui, S. Whitelam and H. Zheng, *Science*, 2012, **336**, 1011–1014.
44 M. Meyns, N. G. Bastus, Y. Cai, A. Kornowski, B. H. Juarez, H. Weller and C. Klinke, *J. Mater. Chem.*, 2010, **20**, 10602–10605.
45 A. R. Studart, J. Studer, L. Xu, K. Yoon, H. C. Shum and D. A. Weitz, *Langmuir*, 2011, **27**, 955–964.
46 K. L. A. Chan, X. Niu, A. J. de Mello and S. G. Kazarian, *Lab Chip*, 2010, **10**, 2170–2174.
47 H. Oyanagi, Z. H. Sun, Y. Jiang, M. Uehara, H. Nakamura, K. Yamashita, L. Zhang, C. Lee, A. Fukano and H. Maeda, *J. Synchrotron Radiat.*, 2011, **18**, 272–279.